



Research paper

Transcritical pressure Organic Rankine Cycle (ORC) analysis based on the integrated-average temperature difference in evaporators

Chao Yu, Jinliang Xu^{*}, Yasong Sun

The Beijing Key Laboratory of Multiphase Flow and Heat Transfer for Low Grade Energy Utilizations, North China Electric Power University, Beijing 102206, PR China

ARTICLE INFO

Article history:

Received 24 June 2014

Received in revised form

12 October 2014

Accepted 11 November 2014

Available online 20 November 2014

Keywords:

Organic Rankine Cycle

Integrated-average temperature difference

Exergy destruction

Thermal match

ABSTRACT

Integrated-average temperature difference (ΔT_{ave}) was proposed to connect with exergy destruction (I_{eva}) in heat exchangers. Theoretical expressions were developed for ΔT_{ave} and I_{eva} . Based on transcritical pressure ORCs, evaporators were theoretically studied regarding ΔT_{ave} . An exact linear relationship between ΔT_{ave} and I_{eva} was identified. The increased specific heats versus temperatures for organic fluid protruded its $T-Q$ curve to decrease ΔT_{ave} . Meanwhile, the decreased specific heats concaved its $T-Q$ curve to raise ΔT_{ave} . Organic fluid in the evaporator undergoes a protruded $T-Q$ curve and a concaved $T-Q$ curve, interfaced at the pseudo-critical temperature point. Elongating the specific heat increment section and shortening the specific heat decrease section improved the cycle performance. Thus, the system thermal and exergy efficiencies were increased by increasing critical temperatures for 25 organic fluids. Wet fluids had larger thermal and exergy efficiencies than dry fluids, due to the fact that wet fluids shortened the superheated vapor flow section in condensers.

© 2014 Elsevier Ltd. All rights reserved.

1. Introduction

The waste heat resource is vast. The Organic Rankine Cycle (ORC) is one of the good solutions to recover the low grade waste heat [1]. Tchanche et al. [2] listed the operating ORC power plants in the world. The work capacity ranged from 125 kW to 6 MW. Many authors investigated ORCs. The investigations focused on the selection of organic fluids [3–5] and the parameter optimizations [6–12].

The geothermal water or flue gas drives ORCs to generate power or electricity [5]. It is discharged to the environment after it releases heat to ORC system. For such power systems, the objective parameter is the maximum work or the largest utilization degree of the heat source. The temperature of heat carrier fluid is decreased after heat is transferred to ORC. For subcritical pressure ORCs, organic fluid undergoes an isothermal evaporating process to yield large exergy loss, deteriorating ORC performance. Alternatively, supercritical pressure ORCs increase organic fluid temperatures continuously during the heating process, resulting in better thermal performance compared with subcritical pressure ORCs [12].

Carbon dioxide (CO_2) is a non-flammability, non-toxic and non-corrosive fluid, having a low critical temperature of 31.3 °C. It can be used in a transcritical power cycle, which has been investigated recently [8,9]. Chen et al. [8] compared CO_2 transcritical power cycle with subcritical pressure R123 ORC. The flue gas had an inlet temperature of 150 °C with a mass flow rate of 0.4 kg/s. It was shown that subcritical pressure ORC had higher thermal efficiency than CO_2 power cycle. But CO_2 power cycle increased the work output due to the raised heat received from the heat source. Cayer et al. [9] investigated transcritical power cycle using CO_2 , ethane and R125 as working fluids at a heat source temperature of 100 °C. The work output reached maximum values by optimizing various parameters.

Transcritical pressure ORCs were investigated in Refs. [12,15–21]. Schuster et al. [12] explored the maximum work output. These authors compared system thermal efficiencies and exergy efficiencies at similar operating conditions between subcritical and transcritical pressure cycles. It was found that transcritical pressure ORCs increased the system thermal efficiencies by 8% compared with subcritical pressure cycles. Zhang et al. [15] performed parameter optimizations for geothermal water driven subcritical and transcritical pressure Rankine cycles. The transcritical pressure cycle with R125 as working fluid could utilize the geothermal water energy to a maximum degree, having better

^{*} Corresponding author. Tel.: +86 10 61772613.
E-mail address: xjl@ncepu.edu.cn (J. Xu).

economic and environmental performances. The hot water temperatures ranged from 80 °C to 100 °C. Vetter et al. [16] compared subcritical and transcritical pressure Rankine cycles driven by the 150 °C geothermal water. The objective parameters included specific net work output, thermal efficiency and heat received from the hot water. Transcritical pressure Rankine cycle with propane as working fluid increased the net work output by 30% compared with subcritical pressure Rankine cycle with isopentane as working fluid. The maximum work output could be reached when the critical temperature of organic fluid was 0.8 times of the geothermal water temperature. Shu et al. [17] proposed a dual-loop ORC to recover the heat of engine flue gas. The net work output and exergy efficiencies were compared between transcritical pressure Rankine cycles with R125, R134a, R218 as working fluids and subcritical pressure Rankine cycles with R124, R134a, R245fa, R600, R600a, R1234yf as working fluids. The transcritical pressure Rankine cycle with R143a as working fluid showed the best cycle performance. Baik et al. [18] compared the work output between transcritical pressure cycle of R125 and subcritical pressure cycle of R134a, R245fa and R152a. The geothermal water temperature was 100 °C. The work output was larger by using the transcritical pressure cycles. Chen et al. [19] identified that transcritical pressure cycles could increase the system thermal efficiencies by 10–30% compared with subcritical pressure cycles. The hottest temperatures of the cycle ranged from 393 K to 473 K. Khennich et al. [20] investigated effects of cycle highest pressures and temperature difference between heat carrier fluid and cycle highest temperature on subcritical and transcritical pressure cycles. The heat source was flue gas, which was regarded as the ideal dry air, having the temperatures of 100 °C, 160 °C and 230 °C, respectively. Subcritical pressure cycle with R141b as working fluid and transcritical pressure cycle with R134a as working fluid were investigated for the 160 °C heat source. Alternatively, both the subcritical and transcritical pressure cycles were studied with R141b as working fluid for the 230 °C heat source. It was found that R141b had the better performance for all the cycles studied. Guo et al. [21] explored the difference between subcritical and transcritical pressure Rankine cycles. When the outlet temperature of heat carrier fluid was relatively low, the transcritical pressure cycles were better than the subcritical pressure cycles regarding thermal efficiencies, exergy efficiencies and work output.

The available studies identified better thermal performance by using transcritical pressure cycles instead of subcritical pressure cycles, due to the better thermal match between heat carrier fluid such as flue gas or geothermal water and organic fluid in evaporators. However, the detailed mechanism needs further studies. One may ask what is the direction to further improve the performance of transcritical pressure cycles? What is the criterion to select suitable working fluids for transcritical pressure cycles? In fact, transcritical pressure cycles are strongly dependent on the heat transfer performance in evaporators. Baik et al. [18] proposed an “average⁰ temperature difference”, which was defined as $1/\Delta T_m = 1/Q_a \int 1/\Delta T dQ$, where Q_a is the total heat transferred by the heat exchanger. When the average temperature difference approaches the pinch temperature difference, the temperature difference along flow path was more uniform. Guo et al. [21] proposed a match coefficient, which was the ratio of exergy destruction assuming that the temperature difference everywhere in the evaporator equals to the pinch temperature difference to real exergy loss in the evaporator.

In this paper, the integrated-average temperature difference was proposed for heat transfer process. It was shown that such temperature difference was directly linked with the exergy destruction to the evaporator. The direction of the ORC cycle

performance was to decrease the temperature difference. The paper was organized as follows. Section 2 described the new parameter and the cycle computation, consisting of three subsections. Section 2.1 shortly described the transcritical power cycle. Section 2.2 described the temperature difference and Section 2.3 described the computation process. Section 3 described the results and discussion, in which Section 3.1 explained why the ORC cycle was mainly influenced by the fluid critical temperatures using the integrated-average temperature difference, Section 3.2 gave the results and data for the computations with 25 organic fluids. The paper gave a guide for the fluid selection to ORCs with respect to efficiencies.

2. The integrated-average temperature difference and the cycle computation

2.1. The ORC cycle

Fig. 1a shows an ORC coupled with a heat source. The flue gas was considered as the heat source, which was characterized by the mass flow rate, m_{gas} , inlet temperature, $T_{gas,in}$, and outlet temperature, $T_{gas,out}$. The analysis of this study was also suitable for other heat carrier fluids such as geothermal water. The flue gas transferred heat to the ORC via an evaporator. Fig. 1b shows the T – s diagram for transcritical pressure ORC. Process 1–2s is an ideal isentropic expansion while 1–2 is a real non-isentropic expansion.

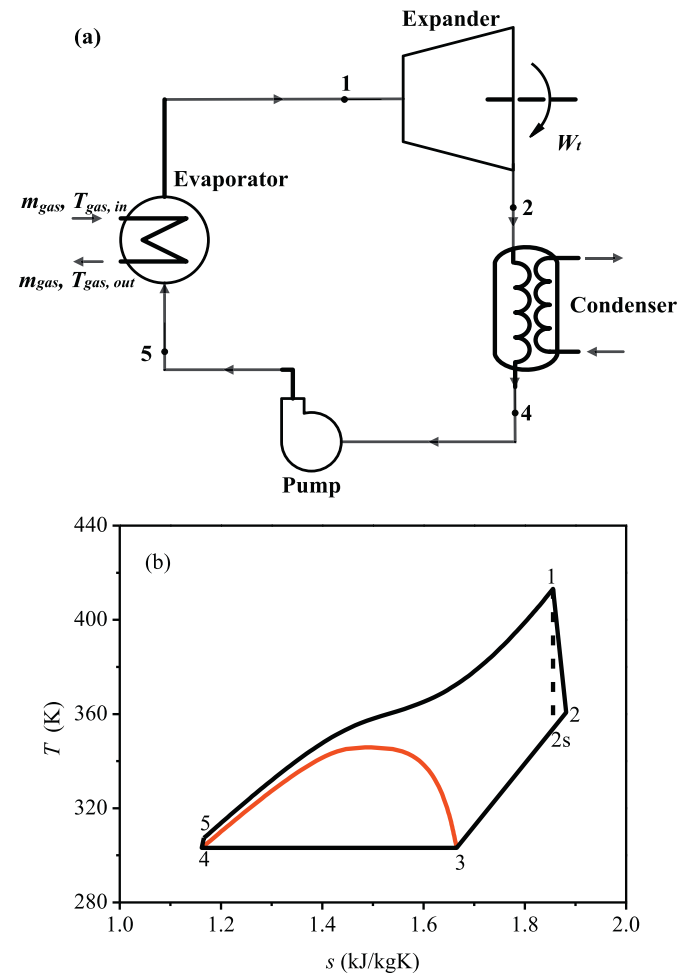


Fig. 1. The transcritical pressure ORCs driven by flue gas.

The organic fluid in the condenser undergoes a superheated vapor state at point 2, a saturated vapor state at point 3 and a saturated liquid state at point 4. It is noted that there is no evaporation heat transfer takes place in the waste heat recovery device at supercritical pressures. However, the flue gas heats the supercritical fluid from a temperature significantly lower than the pseudo-critical temperature to a temperature higher than the pseudo-critical temperature, having the physical properties similar to those of vapor at subcritical pressure. Thus, the term of “evaporator” is still used in this study.

Neglecting pressure drops in the evaporator and condenser, there are two pressures in the ORC with a supercritical pressure of $P_5 = P_1 > P_c$ and a subcritical pressure of $P_2 = P_3 = P_4 < P_c$. Usually, the organic fluid was cooled by air or water at the ambient temperature. Thus, the analysis assumed $T_3 = T_4 = 303.15$ K (30 °C). The condensation pressure was $P_2 = P_3 = P_4 = P_{\text{sat}}(T_3)$.

2.2. The integrated-average temperature difference and the exergy loss

The integrated-average temperature difference was proposed to reflect the integration effect of the heat transfer process in evaporators. Then we explore the internal relationship between the integrated-average temperature difference and the exergy destruction. Such relationship yields the direction to improve the

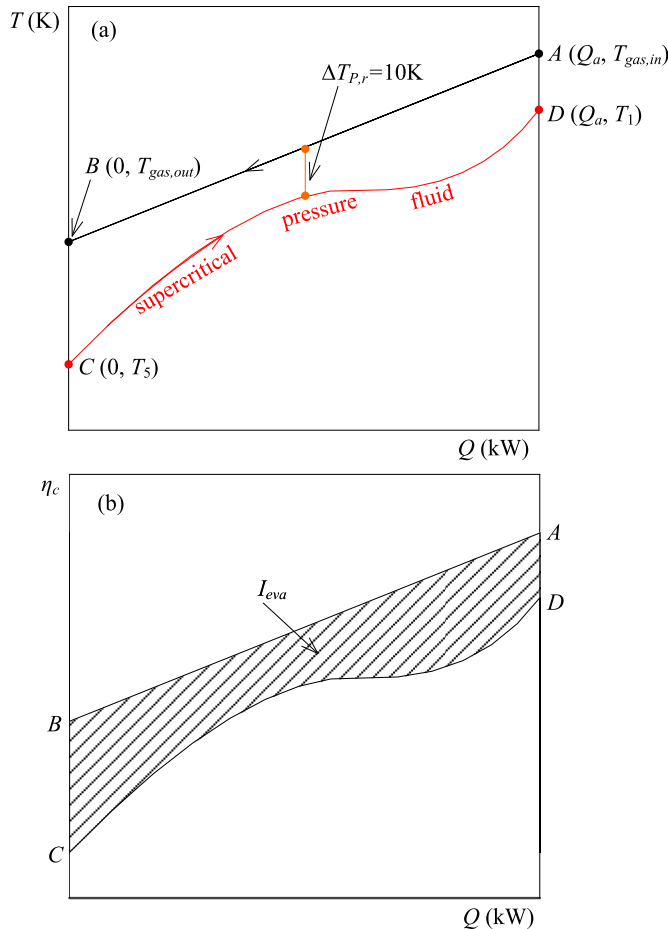


Fig. 2. The T - Q curve of the flue gas and organic fluid (a) and η_c - Q curve in evaporators (b).

ORC performance. Fig. 2a shows the T - Q curve, in which AB is the heat carrier fluid curve, CD is the organic fluid curve. To simplify the analysis, the specific heat of the flue gas (AB curve) was assumed to be constant. However, the slopes of the T - Q curve for the organic fluid were changed due to the varied specific heats versus temperatures. Referring to Fig. 1, the four points in Fig. 2a had the following coordinates: $A(Q_a, T_{\text{gas,in}})$, $B(0, T_{\text{gas,out}})$, $C(0, T_5)$ and $D(Q_a, T_1)$, where Q_a is the total heat released by the flue gas, $T_{\text{gas,in}}$ and $T_{\text{gas,out}}$ are the flue gas temperatures entering and leaving the evaporator, respectively, T_1 and T_5 are the organic fluid temperatures leaving and entering the evaporator, respectively. The integrated-average temperature difference is defined as

$$\Delta T_{\text{ave}} = \frac{\int_0^{Q_a} (T_{\text{gas}} - T_{\text{ORC}}) dQ}{Q_a} \quad (1)$$

where T_{gas} and T_{ORC} are the flue gas temperature and organic fluid temperature, respectively. The integration in the right side of Eq. (1) represents the enclosed area formed by the AB and CD curves. Regarding the flue gas, we have

$$Q_a = m_{\text{gas}} c_{p, \text{gas}} (T_{\text{gas, in}} - T_{\text{gas, out}}) \quad (2)$$

$$Q = m_{\text{gas}} c_{p, \text{gas}} (T_{\text{gas}} - T_{\text{gas, out}}) \quad (3)$$

$$dQ = m_{\text{gas}} c_{p, \text{gas}} dT_{\text{gas}} \quad (4)$$

Regarding the organic fluid, we have

$$Q_a = m_{\text{ORC}} (h_1 - h_5) \quad (5)$$

$$Q = m_{\text{ORC}} (h_{\text{ORC}} - h_5) \quad (6)$$

The specific heat can be a function of temperatures:

$$c_{p, \text{ORC}} = a_0 + a_1 T + a_2 T^2 \quad (7)$$

For simplification purpose, a_2 was neglected. A positive a_1 or negative a_1 correspond to the increased or decreased specific heats versus temperatures, respectively. The enthalpy was expressed as $h = \int_0^T c_{p, \text{ORC}} dT$. Finally, the integrated-average temperature difference was expressed as

$$\Delta T_{\text{ave}} = \frac{1}{2} (T_{\text{gas, in}} + T_{\text{gas, out}}) - \left[\frac{\frac{1}{2} a_0 (T_1 + T_5) + \frac{1}{3} a_1 (T_1^2 + T_1 T_5 + T_5^2)}{a_0 + \frac{a_1}{2} (T_1 + T_5)} \right] \quad (8)$$

For a practical case such as $T_{\text{gas,in}} = 423.15$ K, $T_{\text{gas,out}} = 358.15$ K, $T_1 = 413.15$ K, $T_5 = 307.54$ K, $a_0 = 2.28$ kJ/kg K and $a_1 = 0.02$ kJ/kg K². The calculated ΔT_{ave} was 28.46 K. The following partial derivatives are obtained based on Eq. (8):

$$\frac{\partial \Delta T_{\text{ave}}}{\partial a_0} = \frac{a_1 (T_1 - T_5)^2}{12 \left[a_0 + \frac{a_1}{2} (T_1 + T_5) \right]^2} = c_1 a_1 \quad (9)$$

$$\frac{\partial \Delta T_{\text{ave}}}{\partial a_1} = -\frac{a_0 (T_1 - T_5)^2}{12 \left[a_0 + \frac{a_1}{2} (T_1 + T_5) \right]^2} = -c_1 a_0 \quad (10)$$

On the other hand, the exergy loss within the evaporator is

$$I_{eva} = \int_0^{Q_a} \left(1 - \frac{T_0}{T_{gas}}\right) dQ - \int_0^{Q_a} \left(1 - \frac{T_0}{T_{ORC}}\right) dQ$$

$$= T_0 \int_0^{Q_a} \left(\frac{1}{T_{ORC}} - \frac{1}{T_{gas}}\right) dQ \quad (11)$$

where T_0 is a reference temperature, which is set as the environmental temperature. The final expression of I_{eva} is

$$I_{eva} = \frac{T_0 Q_a \left[a_0 \ln \frac{T_1}{T_5} + a_1 (T_1 - T_5) \right]}{a_0 (T_1 - T_5) + \frac{a_1}{2} (T_1^2 - T_5^2)} - T_0 m_{gas} C_{p, gas} \ln \frac{T_{gas, in}}{T_{gas, out}} \quad (12)$$

Similarly, the partial derivatives of I_{eva} with respect to a_0 and a_1 are

$$\frac{\partial I_{eva}}{\partial a_0} = \frac{\frac{a_1}{2} (T_1 - T_5) \left((T_1 + T_5) \ln \frac{T_1}{T_5} - 2(T_1 - T_5) \right)}{\left[a_0 (T_1 - T_5) + \frac{a_1}{2} (T_1^2 - T_5^2) \right]^2} = c_2 a_1 \quad (13)$$

$$\frac{\partial I_{eva}}{\partial a_1} = \frac{\frac{1}{2} a_0 (T_1 - T_5) \left(2(T_1 - T_5) - (T_1 + T_5) \ln \frac{T_1}{T_5} \right)}{\left[a_0 (T_1 - T_5) + \frac{a_1}{2} (T_1^2 - T_5^2) \right]^2} = -c_2 a_0 \quad (14)$$

Because c_1 and c_2 are positive, Eqs. (9) and (13) show that both $\partial \Delta T_{ave} / \partial a_0$ and $\partial I_{eva} / \partial a_0$ had the sign of a_1 , Eqs. (10) and (14) show that both $\partial \Delta T_{ave} / \partial a_1$ and $\partial I_{eva} / \partial a_1$ had the sign of $-a_0$. We note that a_0 is usually positive, a_1 is the gradient of specific heat variation with respect to temperature. The negative sign of $\partial \Delta T_{ave} / \partial a_1$ and $\partial I_{eva} / \partial a_1$ indicate that both ΔT_{ave} and I_{eva} are decreased with increases in a_1 . The above deduction had the following expectations:

- Effect of a_1 :** For $a_1 = 0$, the CD curve in Fig. 2a is linear, which can be taken as a reference case. The positive a_1 indicates the increased specific heats from point C to D. The CD curve should be protruding to approach the line AB, reducing the enclosed area ABCD, under which the integrated-average temperature difference is decreased and the exergy destruction is less. The negative a_1 indicates the decreased specific heats from point C to D. The CD curve should be concaved to recede from the line AB, under which the integrated-average temperature difference is increased and the exergy destruction is large.
- Effect of a_0 :** For $a_1 < 0$, increase of a_0 reduces ΔT_{ave} and I_{eva} . Alternatively, for $a_1 > 0$, increase of a_0 increases ΔT_{ave} and I_{eva} .
- Always, I_{eva} and ΔT_{ave} share the same change trend.

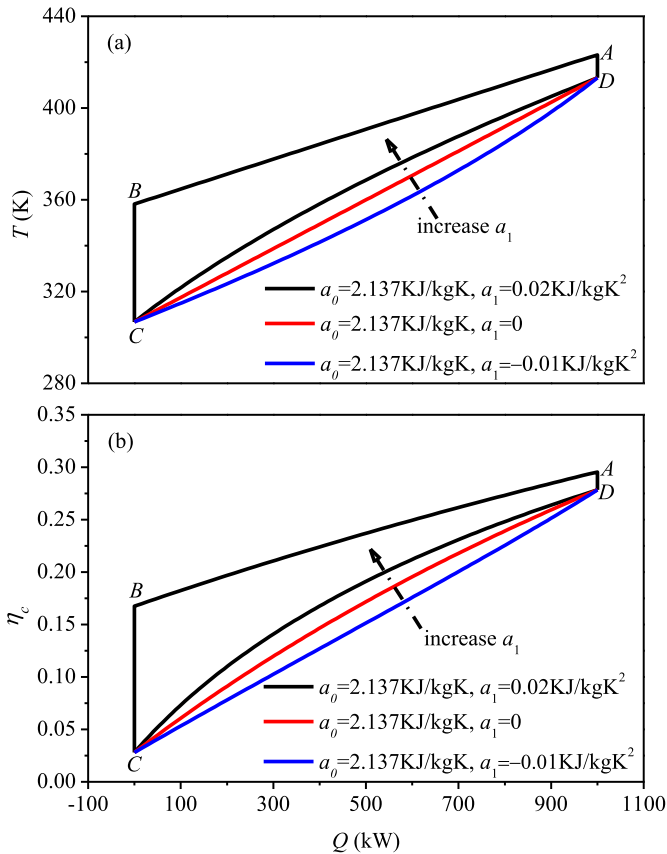


Fig. 3. The T - Q and η_c - Q curves for heat carrier fluid and organic fluid at fixed a_0 (for organic fluid, black curve had $C_{p,5} = 2.137$ kJ/kg K, $C_{p,1} = 4.273$ kJ/kg K, $a_0 = 2.137$ kJ/kg K, $a_1 = 0.02$ kJ/kg K²; red curves had $C_{p,5} = 2.137$ kJ/kg K, $C_{p,1} = 2.137$ kJ/kg K, $a_0 = 2.137$ kJ/kg K, $a_1 = 0$; blue curves had $C_{p,5} = 2.137$ kJ/kg K, $C_{p,1} = 1.068$ kJ/kg K, $a_0 = 2.137$ kJ/kg K, $a_1 = -0.01$ kJ/kg K²). (For interpretation of the references to colour in this figure legend, the reader is referred to the web version of this article.)

Fig. 2b shows the exergy temperature ($\eta_c = 1 - T_0/T$) versus the heat power Q . Figs. 3–4 verified the above findings by plotting the curves at various combinations of a_0 and a_1 , in which Fig. 3 verified the conclusion 1 and Fig. 4 verified the conclusion 2. Both Figs. 3 and 4 verified the conclusion 3. Figs. 3–4 are the numerical tests. The practical applications can be found in heat transfer with supercritical pressure organic fluids. It was found that the integrated-average temperature difference could reflect the change of the exergy destruction in heat exchangers. The ORC performance improvement is to reduce the integrated-average temperature difference to decrease the exergy destruction in evaporators. This is because the evaporator contributed much percentage of the total exergy destruction in ORCs [13,14,22].

It is noted that the linear variation of specific heats versus temperatures may be suitable for most subcritical pressure fluids. For fluids at supercritical pressure the specific heats are sharply changed versus temperatures near the pseudo-critical temperature region. Thus, a more general expression of the integrated-average temperature difference is

$$\Delta T_{ave} = \frac{m_{gas} \int_{T_{gas, out}}^{T_{gas, in}} C_{p, gas} T_{gas} dT_{gas} - m_{ORC} \int_{T_5}^{T_1} C_{p, ORC} T_{ORC} dT_{ORC}}{Q_a} \quad (15)$$

where m_{gas} and m_{ORC} are determined based on Eqs. (2) and (5), respectively. Equation (15) is correct even for varied specific heats versus temperatures for flue gas.

There are several temperature differences defined in thermodynamics or heat transfer textbooks. The logarithmic-mean-temperature-difference is defined as

$$\Delta T_m = \frac{\Delta T_{max} - \Delta T_{min}}{\ln \frac{\Delta T_{max}}{\Delta T_{min}}} \quad (16)$$

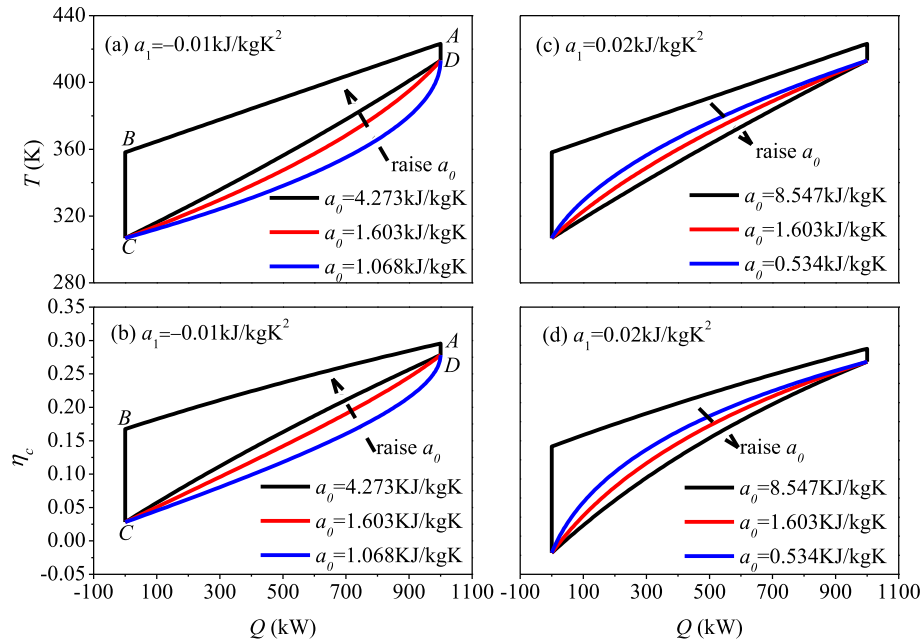


Fig. 4. The T - Q and η_c - Q curves for heat carrier fluid and organic fluid at fixed a_1 (for organic fluid in (a) and (b): black curve had $C_{p,5} = 4.273$ kJ/kg K, $C_{p,1} = 3.209$ kJ/kg K, $a_0 = 4.273$ kJ/kg K, $a_1 = -0.01$ kJ/kg K²; red curves had $C_{p,5} = 1.603$ kJ/kg K, $C_{p,1} = 0.539$ kJ/kg K, $a_0 = 1.603$ kJ/kg K, $a_1 = -0.01$ kJ/kg K²; blue curves had $C_{p,5} = 1.068$ kJ/kg K, $C_{p,1} = 0.0042$ kJ/kg K, $a_0 = 1.068$ kJ/kg K, $a_1 = -0.01$ kJ/kg K²; for organic fluid in (c) and (d): black curve had $C_{p,5} = 8.547$ kJ/kg K, $C_{p,1} = 10.675$ kJ/kg K, $a_0 = 8.547$ kJ/kg K, $a_1 = 0.02$ kJ/kg K²; red curves had $C_{p,5} = 1.603$ kJ/kg K, $C_{p,1} = 3.731$ kJ/kg K, $a_0 = 1.603$ kJ/kg K, $a_1 = 0.02$ kJ/kg K²; blue curves had $C_{p,5} = 0.534$ kJ/kg K, $C_{p,1} = 3.196$ kJ/kg K, $a_0 = 0.534$ kJ/kg K, $a_1 = 0.02$ kJ/kg K²). (For interpretation of the references to colour in this figure legend, the reader is referred to the web version of this article.)

Referring to Fig. 2a,

$$\begin{aligned} \Delta T_{\max} &= \max[(T_{\text{gas, in}} - T_1), (T_{\text{gas, out}} - T_5)], \Delta T_{\min} \\ &= \min[(T_{\text{gas, in}} - T_1), (T_{\text{gas, out}} - T_5)] \end{aligned} \quad (17)$$

Equation (16) is only useful for the heat transfer area estimation and it has no any connection with the exergy destruction in heat exchangers. Many references used the temperature difference at the pinch location, which is recorded as $\Delta T_p = \min(T_{\text{gas}} - T_{\text{ORC}})$. Because the pinch occurs at a specific location, it definitely cannot reflect the integration effect of the heat transfer process over the whole flow length.

2.3. The cycle computation

This paper fully coupled the transcritical pressure ORC with the flue gas heat source. The flue gas inlet temperature ($T_{\text{gas, in}}$) was fixed as 423.15 K (150 °C). The outlet temperature after it released the heat to ORC ($T_{\text{gas, out}}$) was 358.15 K (85 °C), ensuring the vapor condensation in flue gas not occurring so that the tube material corrosion did not happen. That is to say, the 85 °C temperature is usually above the dew point temperature of the flue gas. The mass flow rate of the flue gas is adapted to have the total heat received by the ORC system was 1000 kW (1 MW). The cycle computation needs to determine a set of pressures, temperatures, enthalpies along the ORC loop. The following steps were followed:

- 1. Determination of the CD curve** (see Fig. 2a): The organic fluid temperature leaving the evaporator, T_1 , was $T_1 = T_{\text{gas, in}} - 10$ K. A pressure of P_1 was assumed. The enthalpy is $h_1 = f(P_1, T_1)$. The mass flow rate of the organic fluid was decided by Eq. (5), in which h_5 is the enthalpy at the evaporator inlet of the organic fluid. Then the curve CD was determined, having ΔT_{ave} and I_{eva} values.
- 2. Parameters across the condenser:** Regarding Fig. 1b, the line 3–4 had the temperature of $T_3 = T_4 = 303.15$ K to have

$P_2 = P_3 = P_4 = P_{\text{sat}}(T_3)$. The curve 2–2s–3 had the superheated vapor state and the line 3–4 had the saturated vapor condensation in the condenser. The isentropic expansion process 1–2s determined the point 2s. The isentropic efficiency of the expander (η_{exp}) located the point 2.

- 3. Parameters across the pump:** The isentropic efficiency of the pump (η_p) determined the point 5. Up to now, the whole cycle parameters were determined.
- Steps 1–3 were repeated for a set of pressures. For each organic fluid, there is an optimized pressure at which the system thermal efficiency was maximum and the exergy destruction was minimum.
- Steps 1–4 were repeated for a set of organic fluids with their critical temperatures from low to high.

The cycle computations need several assumptions, which were reasonable and they are described as follows: (1) The pressure difference over the ORC system equals to the pressure drop across the expander inlet and outlet. Pressure drops in other components were neglected. (2) The pinch temperature difference in the evaporator was 10 K, i.e., $\Delta T_{p,r} = 10$ K. The too small pinch temperature difference was difficult to be fulfilled for practical engineering applications. (3) The turbine (or called expander) and pump isentropic efficiencies were 0.75. Chacartegui et al. [23] investigated carbon dioxide based cycles for central receiver solar power plants using a turbine efficiency of 0.87. Cayer et al. [9] analyzed a carbon dioxide transcritical power cycle with a turbine efficiency of 0.8 using a low temperature source. The recent study by Lemort et al. [24] shows that a practical expander may have the isentropic efficiency in the range of 0.6–0.7, significantly lower than those assumed in the literature. Thus, the present paper assumes the isentropic efficiency of 0.75 for the expander.

After all the state parameters in an ORC were determined, the pumping power, turbine (expander) power and thermal efficiency were calculated as

$$W_p = m_{\text{ORC}}(h_5 - h_4) \quad (18)$$

$$W_t = m_{\text{ORC}}(h_1 - h_2) \quad (19)$$

$$\eta_t = \frac{W_t - W_p}{Q_a} \quad (20)$$

Because the computations were performed for constant Q_a , the thermal efficiency was directly proportional to the net power output (see Eq. (20)). The computations of used exergy and exergy efficiency for each component were based on Mago et al. [25] and Tchanche et al. [26]. The detailed expressions are listed in Table 1. The exergy efficiency is defined as the used exergy divided by the available exergy. The system used exergy and available exergy are the sum of the values for each component. The physical properties of the working fluids were computed using the NIST software. The pressure of $P_0 = 0.1$ MPa and $T_0 = 293.15$ K were set as the reference state. The inlet and outlet temperatures of cooling water were 293.15 K and 298.15 K, respectively.

3. Results and discussion

3.1. Effect of critical temperatures of organic fluids on ORCs explained by ΔT_{ave}

We explained why the ORC performance is influenced by critical temperatures of organic fluids. We compared ORCs using two different fluids with one having a low T_c and the other having a relatively higher T_c . Fig. 5 presented results with R32 as working fluid, having $T_c = 351.26$ K, which is lower by 72 K than $T_{\text{gas,in}}$. The pressure was $P_1 = 6.5$ MPa. Fig. 5a shows specific heats versus temperatures, in which $T_{\text{gas,in}}$, the operating points C and D were marked ($T_5 = 307.54$ K at point C and $T_1 = 413.15$ K at point D). Point M was identified as the pseudo-critical temperature, T_{pc} , being 356.90 K at $P_1 = 6.5$ MPa. The specific heat at T_{pc} reached maximum. Interfaced at $T = T_{\text{pc}}$, C_p displayed two regions of CM and MD, behaving increased and decreased specific heats versus temperatures, respectively. Fig. 5b shows that ABCD area consisted of a black shaded area BCMM' and a red shaded area AM'MD. For curve CD, the slopes are $\partial T/\partial Q = 1/m_{\text{ORC}}C_p$, ORC, which are decreased in CM region and increased in MD region. Thus, the specific heat increment region caused protruding curve CD to approach the heat source line AB. On the other hand, the specific heat decrease region yielded concaved curve MD to recede from the heat source line AB. The transition point M had $\partial^2 T/\partial Q^2 = 0$. The computations for R32 are well consistent with the theoretical analysis and numerical tests shown in Section 2.2. Fig. 5c shows the T–S cycle curve. The cycle 12,345 behaved the trapezoid shape, which was not a perfect one.

Because the ABCD area is proportional to the integrated-average temperature difference at constant Q_a ($S_{\text{ABCD}} = \Delta T_{\text{ave}} \cdot Q_a$), the ORC cycle improvement should decrease the ABCD area. Based on Fig. 5, the decrease of ABCD area should elongate the specific heat increment region CM in which the BCMM' area is slim due to the protruded CM curve, but shorten the specific heat decrease region MD in which the AM'MD area is fat due to the concaved MD curve. Usually, T_{pc} at point M follows the T_c change if P_1 does not deviate from the fluid critical pressure (P_c) too much. In summary, the cycle improvement should shift the fluid critical state point to right so that the specific heat increment section is elongated. It is perfect that the fluid critical temperature approaches the flue gas inlet temperature ($T_{\text{gas,in}}$).

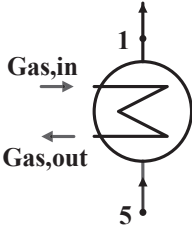
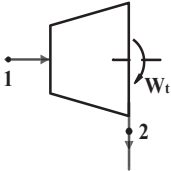
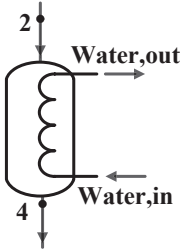
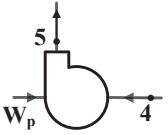
The above analysis was thoroughly verified by Fig. 6 for R152a, in which T_c is 386.41 K, which is only 37 K lower than $T_{\text{gas,in}}$. The specific heat increment region CM contributed longer than the specific heat decrease region MD (see Fig. 6a). Indeed, the ABCD area in Fig. 6b is slim compared with that in Fig. 5b. By raising the fluid T_c , ΔT_{ave} was decreased by 29% to 23.0 K in Fig. 6b, compared with 32.4 K in Fig. 5b. Meanwhile, I_{eav} was decreased by 29%–49.5 kW in Fig. 6, compared with 69.6 kW in Fig. 5. That is to say, ΔT_{ave} and I_{eva} were changed at the same ratio. Fig. 6c shows a perfect triangle cycle to indicate a much improved cycle performance, due to better thermal match between flue gas and organic fluid in the evaporator. Besides, because the fluid envelop curve (red curve) (in web version) was shifted to right due to the raised T_c , point 3 was slightly beyond the $T_{\text{gas,in}}$ point, the superheated vapor flow section was shortened to improve the condenser performance by comparing Fig. 6c with Fig. 5c.

Fig. 7 shows exergy destructions contributed by each component of the ORC system. Fig. 7a shows that for R32 having a lower T_c , the total exergy destruction was 137.71 kW. The evaporator contributed about half of the total exergy destructions. The expander and condenser were the second and third largest contributors. Using higher T_c fluid shown in Fig. 7b significantly changed the exergy destruction distributions. The total exergy destruction was decreased to 120.10 kW. The evaporator, expander and condenser contributed 41.56%, 35.51% and 16.92%, respectively. The difference between evaporator and expander was weakened due to significantly decreased exergy destruction of the evaporator.

3.2. The ORC performances dependent on critical temperatures of organic fluids

Fig. 8 shows system thermal efficiencies (η_t), exergy efficiencies ($\eta_{\text{e,sys}}$), integrated-average temperature difference (ΔT_{ave}) and exergy destruction in the evaporator (I_{eva}) versus critical temperatures of various fluids. Each data point represented a fluid. Our

Table 1
Exergy analysis for each ORC component.

Component	Evaporator	Turbine	Condenser	Pump
Schematic				
Used exergy	$E_1 - E_5$	W_t	$E_{\text{water,out}} - E_{\text{water,in}}$	$E_5 - E_4$
Available exergy	$E_{\text{gas,in}} - E_{\text{gas,out}}$	$E_1 - E_2$	$E_2 - E_4$	W_p

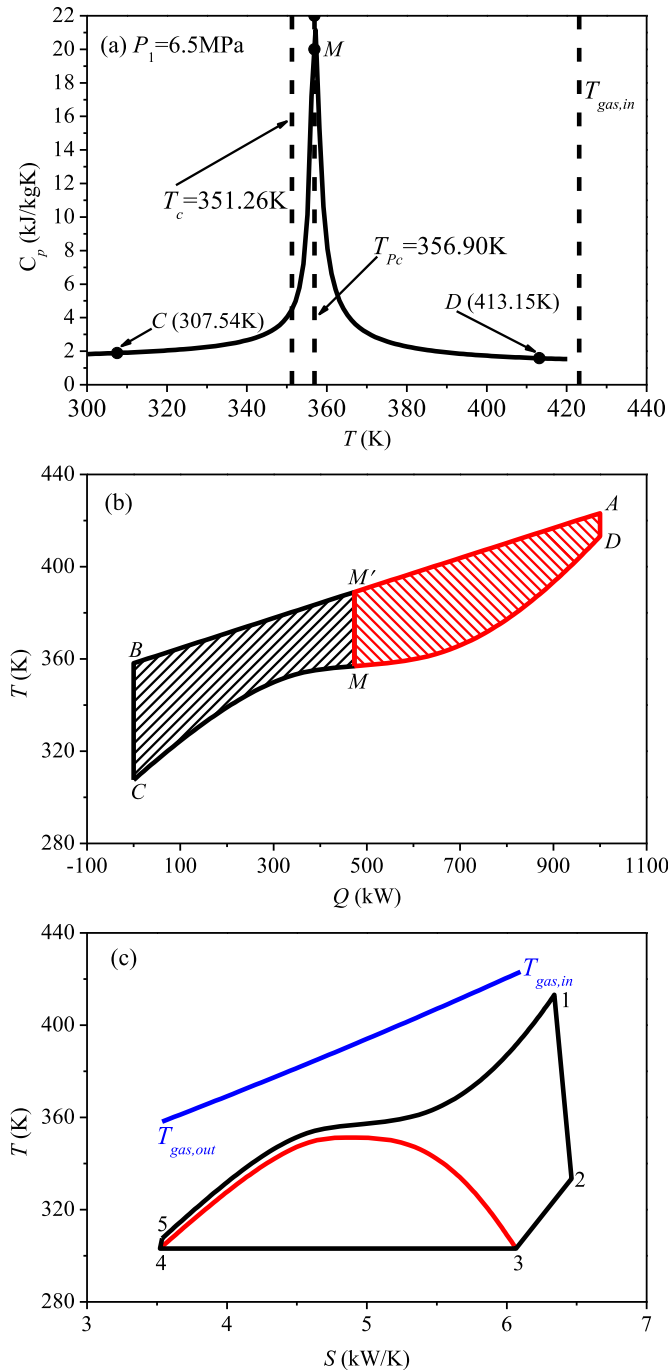


Fig. 5. The C_p , T - Q and T - S curves for R32 at the pressure $P_1 = 6.5$ MPa.

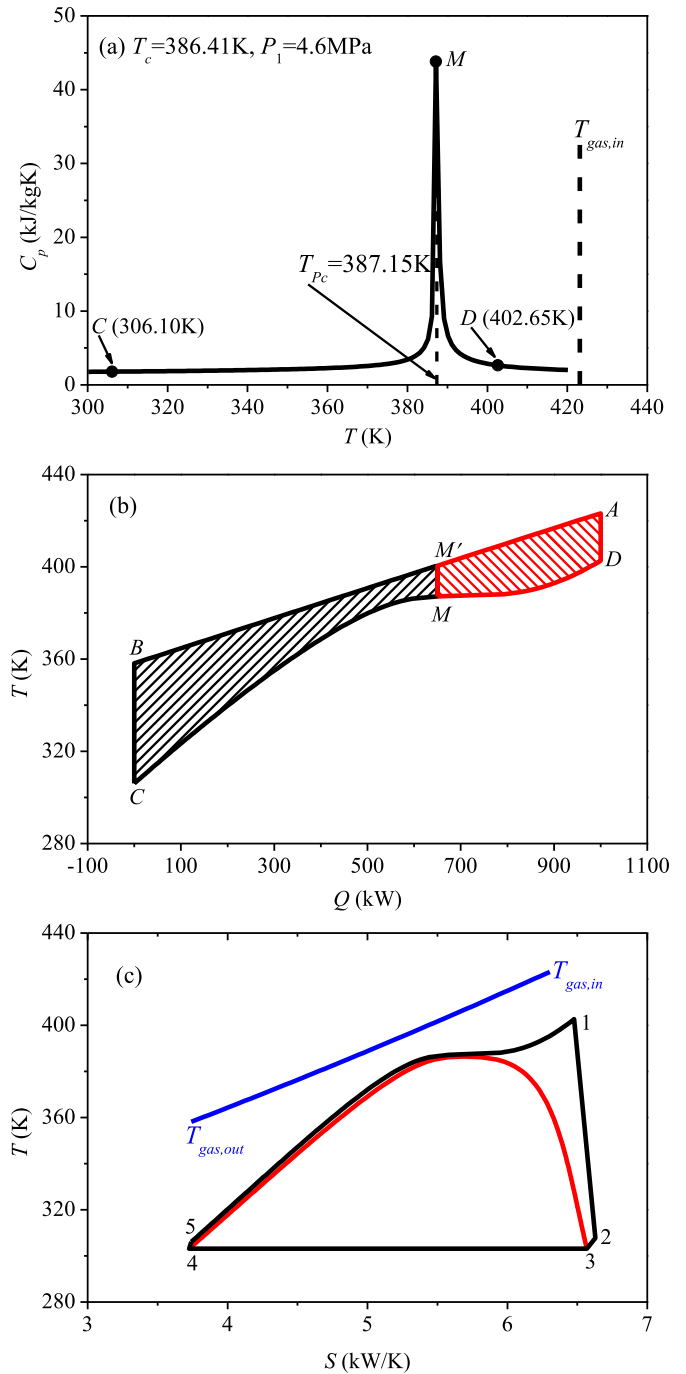


Fig. 6. The C_p , T - Q and T - S curves for R152a at the pressure $P_1 = 4.6$ MPa.

previous studies [28] showed that for fluid critical temperatures significantly lower than the flue gas inlet temperature, $T_{gas,in}$, the pinch was located at the evaporator outlet. This is because the T - Q curve of organic fluid behaved concave shape to recede from the T - Q curve of heat source. When critical temperatures gradually approached to $T_{gas,in}$, the pinch temperature shifted to somewhere between evaporator inlet and outlet, due to the protruding T - Q curve of organic fluid. The exact pinch location was dependent on the operating pressure P_1 in the evaporator. Fig. 8 shows results at the pinch temperature difference ($\Delta T_{p,r}$) of 10 K. The cycle computation given in Section 2.3 shows varied thermal efficiencies versus P_1 for a specific organic fluid, i.e. $\eta_t = f(P_1)$, noting that the

thermal efficiency is proportional to net power output, W_{net} . Our computations were performed at specific Q_a . Each data point in Fig. 8 was optimized with respect to a set of pressures for a specific organic fluid. The largest thermal and exergy efficiencies happened for R161, having T_c of 375.3 K, which was 0.88 times of $T_{gas,in}$ ($T_{c,R161}/T_{gas,in} = 0.88$). ΔT_{ave} and I_{eva} were smallest among the 25 organic fluids. Ref. [16] concluded that the largest efficiency happened for fluid having T_c of 0.8–0.9 times of the heat source temperature.

Ref. [27] classified organic fluids as dry fluids ($\xi > 1$ J/kgK²), wet fluid ($\xi < -1$ J/kgK²), and isentropic fluid (-1 J/kgK² $< \xi < 1$ J/kgK²), here ξ was the slope of the T - s curve ($\xi = \partial s/\partial T$). The present study identified that wet fluids had larger thermal efficiencies than dry

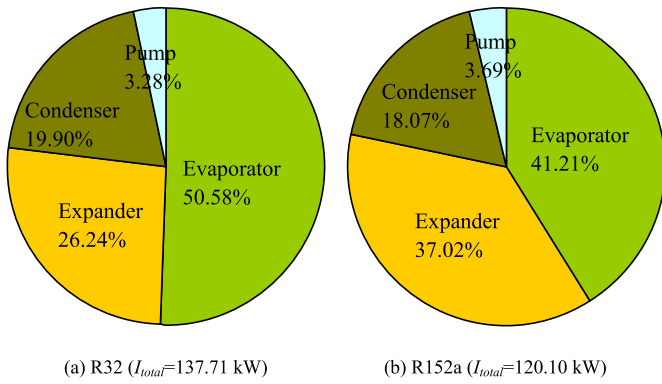


Fig. 7. Exergy destruction by each component of the ORC, (a) for R32 and (b) for R152a.

fluids when they had similar critical temperatures. Among the quasi-isentropic fluids, the thermal efficiencies for fluids having dryness $\xi < 0.55 \text{ J/kg K}^2$ had larger thermal efficiencies. Thus, the fluids with $\xi < 0.55 \text{ J/kg K}^2$ were classified to be quasi-wet fluids. The fluids with $\xi > 0.55 \text{ J/kg K}^2$ had relatively lower thermal efficiencies, which could be treated as quasi-dry fluids. The data points for quasi-wet fluids were connected with each other in Fig. 8. R161 had the maximum system thermal and exergy efficiencies, corresponding to the lowest ΔT_{ave} and I_{eva} . Before the maximum efficiency point, thermal and exergy efficiencies were increased with fluid critical temperatures, majorly due to elongated specific heat increment region in which $T-Q$ curves were protruded to approach $T-Q$ curve of the heat source, with increases in T_c . The detailed analysis was given in Section 3.1. Beyond the maximum efficiency point for R161, thermal and exergy efficiencies were only slightly decreased. The high T_c fluids were also acceptable from the efficiency point of view.

Fig. 8 had solid symbols for quasi-dry fluids of R218, R115, R227ea, perfluorobutane and RC318. These fluids had lower efficiencies compared with quasi-wet fluids when critical temperatures were similar. At similar critical temperatures, dry fluids and wet fluids had similar integrated-average temperature difference and exergy destruction in the evaporator. The difference in efficiencies lied in the condenser performance. Fig. 9 explored the reason. ΔT_{ave} and I_{eva} for R236fa were close to those for RC318, respectively. However, due to different dryness of the two fluids, the superheated vapor flow section in condenser was different. The dry fluid RC318 elongated the superheated vapor flow length in

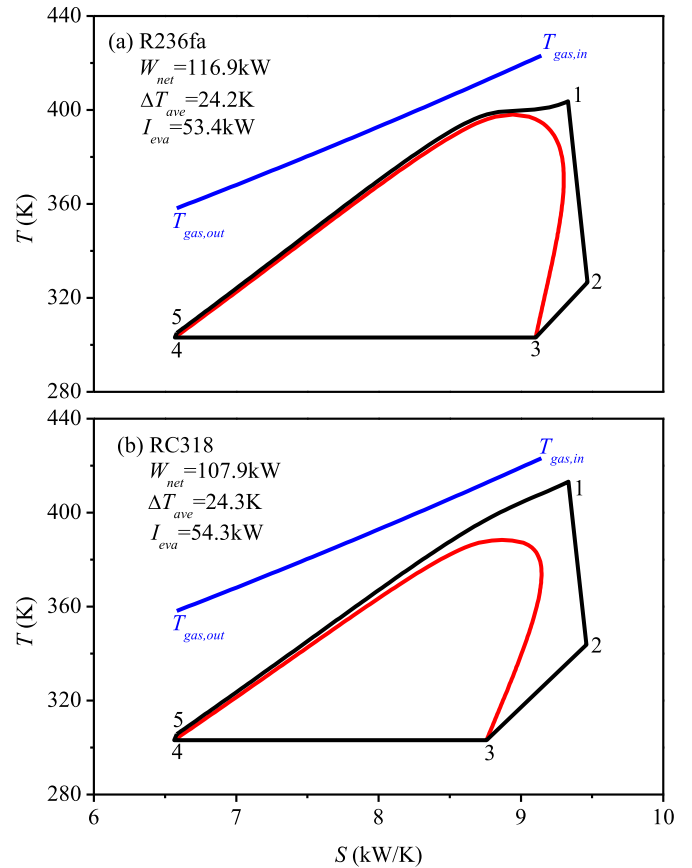


Fig. 9. The cycle difference between quasi-isentropic fluid (R236fa, $T_c = 398.07 \text{ K}$) and dry fluid (RC318, $T_c = 388.38 \text{ K}$).

condenser (process 2–3 in Fig. 9b). This increased the exergy destruction in condenser to form a trapezoid cycle (see Fig. 9b). Meanwhile, the cycle shown in Fig. 9a approached a triangle cycle for R236fa.

More attention was paid to system thermal efficiencies, or net power output because Q_a was fixed. Fig. 10 shows η_t versus ΔT_{ave} and I_{eva} . The general trend was the decreased η_t versus ΔT_{ave} and I_{eva} , reflecting the major exergy destruction contributed by

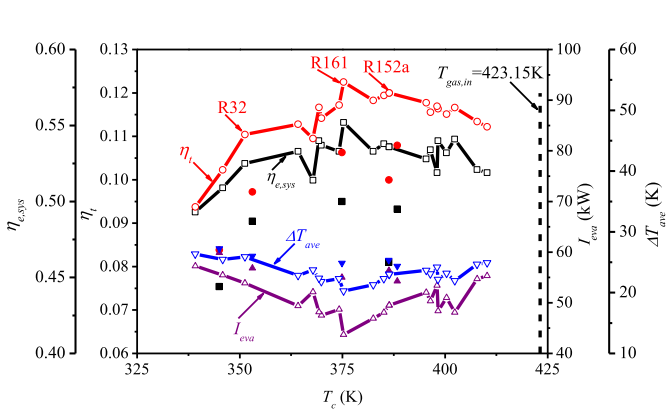


Fig. 8. The η_t , $\eta_{e,sys}$, I_{eva} and ΔT_{ave} versus T_c ($T_{gas,in} = 423.15 \text{ K}$, $T_{gas,out} = 358.15 \text{ K}$, $Q_a = 1 \text{ MW}$, $\Delta T_{pr} = 10 \text{ K}$; fluids with $\xi < 0.55 \text{ J/kgK}^2$: R125, R143a, R32, propylene, R1234yf, R22, propane, R134a, R161, R1234ze, R12, R152a, R124, trifluoroiodomethane, R236fa, cyclopropane, dimethylether, propyne, isobutane, R142b; solid symbols for fluids with $\xi > 0.55 \text{ J/kg K}^2$: R218, R115, R227ea, perfluorobutane, RC318).

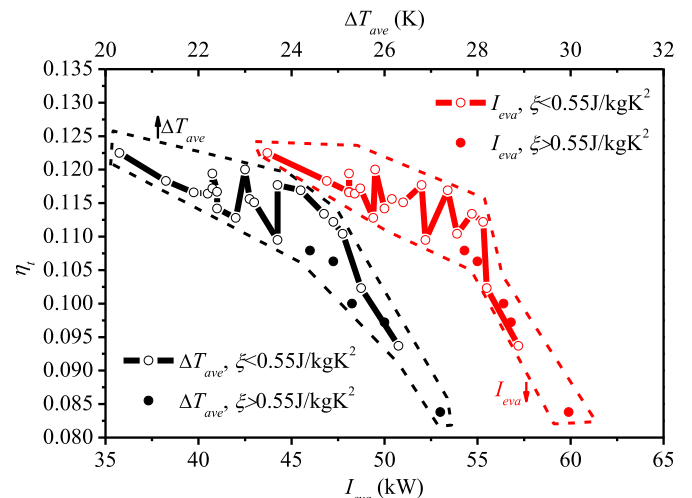


Fig. 10. Thermal efficiency η_t versus ΔT_{ave} and I_{eva} .

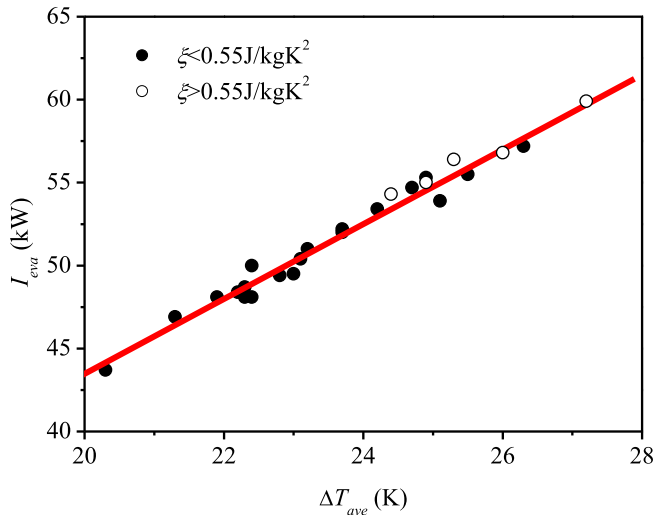


Fig. 11. The linear relationship between I_{eva} and ΔT_{ave} .

evaporator. Decrease ΔT_{ave} and I_{eva} in evaporator led to improved system performance. On the other hand, the slightly decreased thermal efficiencies with quasi-dry fluids (solid symbols) reflected the effect of fluid dryness on the condenser to influence system performance.

Fig. 11 shows perfect linear relationship between ΔT_{ave} and I_{eva} . The integrated-average temperature difference was represented by enclosed area of heat source and organic fluid. ΔT_{ave} reflects the integration effect of the heat transfer process. Any other temperature difference such as pinch temperature difference or logarithmic-mean-temperature-difference cannot do this because they are only determined at specific points in the flow path. It is noted that the integrated-average temperature difference was also useful for other heat transfer processes.

Finally, we gave cycle computation data in Table 2, in which fluids, T_c , P_1 , T_1 , I_{eva} , ΔT_{ave} , η_b , $\eta_{e,sys}$ and ξ were listed one by one. The pressure P_1 was optimized to have the maximum efficiency for a specific fluid. Results were given for 25 fluids, including dry, wet and isentropic fluids, represented by three colors. Table 2 helps readers to select suitable working fluids for transcritical pressure ORCs for the heat source temperature of about 150 °C. It is noted that this paper only paid attention to the system efficiencies. The selection of working fluids should also consider a set of factors such as environmental effect, safety, etc. These factors are beyond the scope of this paper.

3.3. Comparison with other studies

Here we compared the integrated-average temperature difference with the pinch temperature difference and the logarithmic mean temperature difference (LMTD). The pinch point analysis was first proposed by Linnhoff in 1978 for the heat exchanger network synthesis (HENS) [29]. Based on the energy conservation principle, the pinch point analysis determines the cooling load and heating load to satisfy the energy target. The purpose of pinch point analysis was to design suitable heat recovery scheme. Furman & Sahinidis [29] reviewed the development of the pinch point analysis. Morar & Agachi [30] summarized the progress of the heat integration for heat exchanger network in the period of 1975–2008. Friedler [31] discussed the process integration for energy saving and pollution reduction. Even though the pinch point analysis is mature up to now, new progress has been made recently. Bonhivers et al. [32,33] proposed the “bridge analysis”, providing more detail about heat savings modifications. The analysis bridges existing

heaters and coolers. Tan et al. [34] pointed out that most of the established methods for utility targeting in a heat exchanger network (HEN) are mainly focusing on fixed stream conditions, where the flow rate, heat capacity, supply and target temperatures are fixed. However, in the process industries, the stream conditions are not fixed. Therefore, the established HEN targeting methods cannot be directly applied to locate the hot and cold utility targets for HEN problem with varying flow rates and temperatures. Thus, a revised floating pinch method which uses binary variables to quantify the stream locations on the composite curves, was presented to identify the minimum utilities targets.

The integrated-average temperature difference differs from the pinch point analysis in the following ways. The pinch point analysis considers a heat exchanger network, but the integrated-average temperature difference deals with a specific heat exchanger. Fundamentally, the pinch point analysis determines the quantity of heat to be recovered and additional heating load and cooling load to be needed for given heat exchanger network. The method only considers the energy balance among various heat exchanger components. The integrated-average temperature difference deals with the loss of the energy grade, having a strong connection with the exergy destruction for a heat transfer process. Finally, the pinch point analysis deals with the constant specific heat of fluid, while the integrated-average temperature difference considers the varied specific heat of fluids.

Now we compare the logarithmic mean temperature difference (LMTD) with the integrated-average temperature difference. It is seen from Fig. 2a that LMTD can be determined when the temperatures at the points of A, B, C and D are given. The LMTD value is independent of the heat transfer route from point A to B for the heat carrier fluid, and from point C to D for the organic fluid. Thus, LMTD is a state parameter and it has nothing to do with the exergy destruction of the evaporator. However, the integrated-average temperature difference is not only related to the temperatures at points of A, B, C and D, but also related to the heat transfer routes from A to B, and from C to D. Thus, it is a process parameter. The heat transfer paths strongly influence the enclosed area of ABCD. This study certified that the enclosed area is proportional to the exergy destruction of the heat exchanger. A smaller enclosed ABCD area corresponds to a smaller exergy destruction in the evaporator. This conclusion cannot be reached by LMTD.

Fig. 12 shows the effect of the heat transfer routes on the evaporator performance, with $T_{gas,in} = 423.15$ K and $T_{gas,out} = 358.15$ K. Both the red and blue curves were heated from $T_5 = 306.9$ K to $T_1 = 413.15$ K. Thus, LMTD was equal to 25.2 K, being identical for R143a and R161. However, different heat transfer routes induce significantly different enclosed area between heat source and organic fluid. The flue gas and R161 fluid formed much smaller enclosed area than the heat source and R143a fluid. The integrated-average temperature difference was 19.8 K for R161 and 32.5 K for R143a. Consequently, R161 constructed the exergy destruction of 42.8 kW but R143a generated the exergy destruction of 70.5 kW. Finally, the ORC with R161 fluid generated 122.7 kW power output. But the power output was only 102.3 kW with R143a fluid. In summary, the integrated-average temperature difference is proportional to the exergy destruction of the evaporator. Thus it determines and influences the cycle power output. This conclusion cannot be reached by LMTD. It is necessary to use the integrated-average temperature difference for ORC analysis.

4. Conclusions

The integrated-average temperature difference (ΔT_{ave}) was presented to quantify the thermal match between heat source and organic fluid in evaporators. It was shown that ΔT_{ave} is directly

Table 2
The computational data for transcritical pressure ORCs.

Fluids	T_c (K)	p_1 (MPa)	T_1 (K)	I_{eva} (kW)	ΔT_{ave} (K)	η_t	$\eta_{e,sys}$	ζ (J/kg·K ²)
R125	339.17	8.5	413.15	57.2	26.3	0.0937	0.493	-0.684
R218	345.02	6.5	413.15	59.9	27.2	0.0838	0.444	0.708
R143a	345.86	7.5	413.15	55.5	25.5	0.1023	0.509	-1.713
R32	351.26	9.0	413.15	53.9	25.1	0.1104	0.525	-5.601
R115	353.10	6.2	413.15	56.8	26.0	0.0972	0.487	0.016
propylene	364.21	6.5	413.15	49.4	22.8	0.1128	0.533	-4.183
R1234yf	367.85	5.5	413.15	52.2	23.7	0.1095	0.514	-0.386
R22	369.30	6.5	413.15	48.1	22.4	0.1167	0.540	-2.396
propane	369.89	6.0	413.15	50.0	22.4	0.1142	0.535	-3.226
R134a	374.21	5.5	413.15	48.7	22.3	0.1172	0.533	-0.961
R227ea	374.90	5.0	413.15	55.0	24.9	0.1063	0.500	0.575
R161	375.30	6.2	413.15	43.7	20.3	0.1225	0.552	-4.163
R1234ze	382.52	4.6	413.15	46.9	21.3	0.1183	0.533	-0.338
R12	385.12	4.3	408.15	48.1	22.3	0.1194	0.538	-0.969
perfluorobutane	386.33	3.5	413.15	56.4	25.3	0.1000	0.460	1.314
R152a	386.41	4.6	402.65	49.5	23.0	0.1200	0.536	-2.411
RC318	388.38	4.0	413.15	54.3	24.4	0.1079	0.495	0.907
R124	395.43	3.8	401.55	52.0	23.7	0.1177	0.528	-0.138
C3FI	396.44	4.1	399.70	50.4	23.1	0.1156	0.534	-0.727
R236fa	398.07	3.3	403.65	53.4	24.2	0.1169	0.519	0.511
cyclopropane	398.30	5.7	400.05	48.4	22.2	0.1164	0.540	-1.521
dimethylether	400.38	5.5	402.40	51.0	23.2	0.1151	0.532	-3.148
propyne	402.38	5.7	403.15	48.1	21.9	0.1166	0.541	-3.17
isobutane	407.81	3.8	410.00	54.7	24.7	0.1134	0.521	-0.419
R142b	410.26	4.2	411.15	55.3	24.9	0.1122	0.519	-0.703

Note: black color represents isentropic working fluids; blue color represents wet fluids; red color represents dry working fluids; ζ were calculated by the formula defined in Ref. [27].

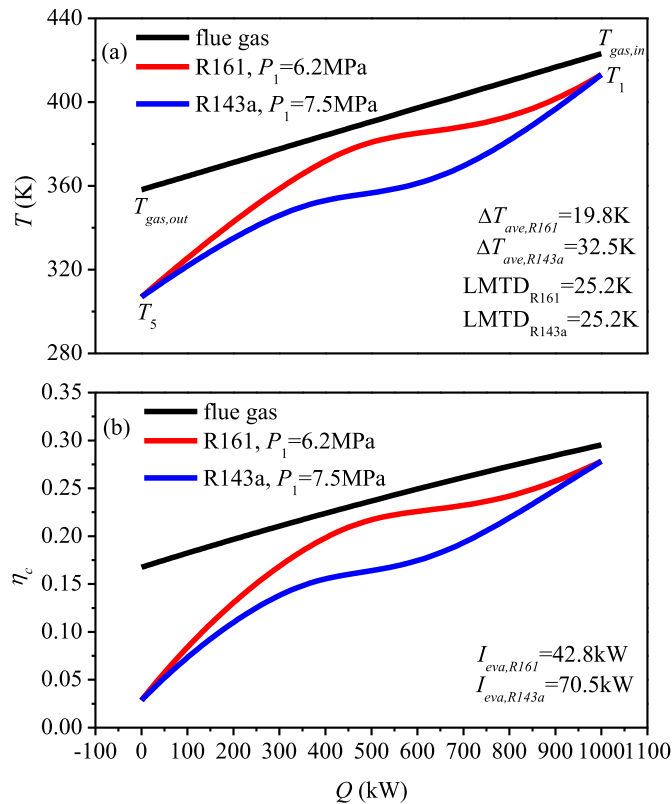


Fig. 12. Influence of the heat transfer routes on the exergy destruction of the evaporator.

proportional to the exergy destruction of evaporators (I_{eva}). The variations of specific heats altered the heat transfer routes to influence ΔT_{ave} and I_{eva} . Evaporators operating at supercritical pressure consisted of a protruded $T-Q$ curve part and a concaved $T-Q$ curve part, interfaced at the pseudo-critical temperature point. The two curve parts corresponded to the specific heat increment section and decrease section, respectively. Higher critical temperature of organic fluid elevated its $T-Q$ curve to approach the heat source $T-Q$ curve, increasing the power output and thermal efficiencies. Totally twenty-five organic fluids were examined based on the integrated-average temperature difference analysis. It was shown that the ORC performance was gradually improved by using organic fluids with increased critical temperatures. The thermal efficiencies of ORCs were larger for wet fluids than for dry fluids. This is because wet fluids shortened the superheated vapor flow section in condensers. This study provides a guide to select organic fluids regarding efficiencies for transcritical pressure ORCs.

Acknowledgements

This work was supported by the Natural Science Foundation of China of International cooperation project (51210011) and the Natural Science Foundation of China (51206043).

References

- [1] D. Wei, X. Lu, Z. Lu, J. Gu, Performance analysis and optimization of organic Rankine cycle (ORC) for waste heat recovery, *Energy Convers. Manag.* 48 (2007) 1113–1119.
- [2] B.F. Tchanche, G. Lambrinos, A. Frangoudakis, G. Papadakis, Low-grade heat conversion into power using organic Rankine cycles – A review of various applications, *Renew. Sustain. Energy Rev.* 15 (2011) 3963–3979.

- [3] H. Chen, D.Y. Goswami, E.K. Stefanakos, A review of thermodynamic cycles and working fluids for the conversion of low-grade heat, *Renew. Sustain. Energy Rev.* 14 (2010) 3059–3067.
- [4] N.A. Lai, M. Wendland, J. Fischer, Working fluids for high-temperature organic Rankine cycles, *Energy* 36 (2011) 199–211.
- [5] B. Saleh, G. Koglbauer, M. Wendland, J. Fischer, Working fluids for low-temperature organic Rankine cycles, *Energy* 32 (2007) 1210–1221.
- [6] F. Ayachi, E.B. Ksayer, A. Zoughaib, P. Neveu, ORC optimization for medium grade heat recovery, *Energy* 68 (2014) 47–56.
- [7] Y. Dai, J. Wang, L. Gao, Parametric optimization and comparative study of organic Rankine cycle (ORC) for low grade waste heat recovery, *Energy Convers. Manag.* 50 (2009) 576–582.
- [8] Y. Chen, P. Lundqvist, A. Johansson, P. Platell, A comparative study of the carbon dioxide transcritical power cycle compared with an organic Rankine cycle with R123 as working fluid in waste heat recovery, *Appl. Therm. Eng.* 26 (2006) 2142–2147.
- [9] E. Cayer, N. Galanis, M. Desilets, H. Nesreddine, P. Roy, Analysis of a carbon dioxide transcritical power cycle using a low temperature source, *Appl. Energy* 86 (2009) 1055–1063.
- [10] J. Sun, W. Li, Operation optimization of an organic Rankine cycle (ORC) heat recovery power plant, *Appl. Therm. Eng.* 31 (2011) 2032–2041.
- [11] S. Karellas, A. Schuster, Supercritical fluid parameters in organic Rankine cycle applications, *Int. J. Thermodyn.* 11 (2008) 101–108.
- [12] A. Schuster, S. Karellas, R. Aumann, Efficiency optimization potential in supercritical Organic Rankine Cycles, *Energy* 35 (2010) 1033–1039.
- [13] T.C. Hung, Waste heat recovery of organic Rankine cycle using dry fluids, *Energy Convers. Manag.* 42 (2001) 539–553.
- [14] Q. Chen, J. Xu, H. Chen, A new design method for Organic Rankine Cycles with constraints of inlet and outlet heat carrier fluid temperatures coupling with the heat source, *Appl. Energy* 98 (2012) 562–573.
- [15] S. Zhang, H. Wang, T. Guo, Performance comparison and parametric optimization of subcritical Organic Rankine Cycle (ORC) and transcritical power cycle system for low-temperature geothermal power generation, *Appl. Energy* (2011) 2740–2754.
- [16] C. Vetter, H.J. Wiemer, D. Kuhn, Comparison of sub- and supercritical Organic Rankine Cycles for power generation from low-temperature/low-enthalpy geothermal wells, considering specific net power output and efficiency, *Appl. Therm. Eng.* 51 (2013) 871–879.
- [17] G. Shu, L. Liu, H. Tian, H. Wei, X. Xu, Performance comparison and working fluid analysis of subcritical and transcritical dual-loop organic Rankine cycle (DORC) used in engine waste heat recovery, *Energy Convers. Manag.* 74 (2013) 35–43.
- [18] Y. Baik, M. Kim, K. Chang, Y. Lee, H. Yoon, A comparative study of power optimization in low-temperature geothermal heat source driven R125 transcritical cycle and HFC organic Rankine cycles, *Renew. Energy* 54 (2012) 78–84.
- [19] H. Chen, D. Goswami, M. Rahman, E. Stefanakos, Converting low-grade heat into power using a supercritical Rankine cycle with zeotropic mixture working fluid. Proceedings of the ASME 2010 4th International Conference on Energy Sustainability. ES2010.
- [20] M. Khennich, N. Galanis, Optimal design of ORC systems with a low-temperature heat source, *Entropy* 14 (2012) 370–389.
- [21] C. Guo, X. Du, L. Yang, Y. Yang, Performance analysis of organic Rankine cycle based on location of heat transfer pinch point in evaporator, *Appl. Therm. Eng.* 62 (2014) 176–186.
- [22] B.F. Tchanche, G. Papadakis, G. Lambrinos, A. Frangoudakis, Fluid selection for a low-temperature solar organic Rankine cycle, *Appl. Therm. Eng.* 29 (2009) 2468–2476.
- [23] R. Chacartegui, J.M.M. Escalona, D. Sánchez, B. Monje, T. Sánchez, Alternative cycles based on carbon dioxide for central receiver solar power plants, *Appl. Therm. Eng.* 31 (2011) 872–879.
- [24] V. Lemort, S. Quoilin, C. Cuevas, J. Lebrun, Testing and modeling a scroll expander integrated into an Organic Rankine Cycle, *Appl. Therm. Eng.* 14–15 (2009) 3094–3102.
- [25] P.J. Mago, K.K. Srinivasan, L.M. Chamra, C. Somayaji, An examination of exergy destruction in organic Rankine cycles, *Int. J. Energy Res.* 32 (2008) 926–938.
- [26] B.F. Tchanche, G. Lambrinos, A. Frangoudakis, G. Papadakis, Exergy analysis of micro-organic Rankine power cycles for a small scale solar driven reverse osmosis desalination system, *Appl. Energy* 87 (2010) 1295–1306.
- [27] B.T. Liu, K.H. Chien, C.C. Wang, Effect of working fluids on organic Rankine cycle for waste heat recovery, *Energy* 29 (2004) 1207–1217.
- [28] J. Xu, C. Liu, Effect of the critical temperature of organic fluids on supercritical pressure Organic Rankine Cycles, *Energy* 63 (2013) 109–122.
- [29] K.C. Furman, N.V. Sahinidis, A critical review and annotated bibliography for heat exchanger network synthesis in the 20th century, *Industrial Eng. Chem. Res.* 41 (2002) 2335–2370.
- [30] M. Morar, P.S. Agachi, Review: Important contributions in development and improvement of the heat integration techniques, *Comput. Chem. Eng.* 34 (2010) 1171–1179.
- [31] F. Friedler, Process integration, modeling and optimization for energy saving and pollution reduction, *Appl. Therm. Eng.* 30 (2010) 2270–2280.
- [32] J.C. Bonhivers, E. Svensson, T. Berntsson, P.R. Stuart, Comparison between pinch analysis and bridge analysis to retrofit the heat exchanger network of a kraft pulp mill, *Appl. Therm. Eng.* 70 (2014) 369–379.
- [33] J.C. Bonhivers, B. Srinivasan, P.R. Stuart, New analysis method to reduce the industrial energy requirements by heat-exchanger network retrofit: Part 1-Concepts, *Appl. Therm. Eng.*, <http://dx.doi.org/10.1016/j.applthermaleng.2014.04.078>.

- [34] Y.L. Tan, D.K.S. Ng, M.M. El-Halwagi, D.C.Y. Foo, Y. Samyudia, Floating pinch method for utility targeting in heat exchanger network (HEN), Chem. Eng. Res. Des. 92 (2014) 119–126.

Nomenclature

a_0 : coefficient in Eq. (7) (kJ/kg K)
 a_1 : coefficient in Eq. (7) (kJ/kg K²)
 a_2 : coefficient in Eq. (7) (kJ/kg K³)
 C_p : specific heat (kJ/kg K)
 c_1 : coefficient in Eqs. (9) and (10)
 c_2 : coefficient in Eqs. (13) and (14)
 E : exergy (kW)
 h : specific enthalpy (kJ/kg)
 I : exergy destruction (kW)
 I_{total} : exergy destruction of all components (kW)
 m : mass flow rate (kg/s)
 P : pressure (MPa)
 Q : heating power (kW)
 Q_a : total heat released by flue gas (kW)
 s : specific entropy (kJ/kg K)
 T : temperature (K)
 W : power (kW)

Greek symbols

ΔT : temperature difference between flue gas and organic fluid (°C or K)

ΔT_m : logarithmic-mean-temperature-difference (°C or K)
 η : efficiency
 η_c : exergy temperature
 ξ : fluid dryness, J/kg K²

Subscripts

0 : reference state
 $1 \sim 5$: points corresponding to Fig. 1
 ave : integrated-average
 c : critical state of organic fluid
 e : exergy
 eva : evaporator
 exp : expander
 gas : flue gas
 in : inlet
 max : maximum value
 min : minimum value
 out : outlet
 ORC : Organic Rankine Cycle or organic fluid
 p : pinch point or pump
 pc : pseudocritical state of organic fluid
 r : requirement
 s : isentropic
 sat : saturation point
 sys : ORC system
 t : turbine
 $water$: cooling water